Research Article | Vol. 25, No. 7 | 3 Apr 2017 | OPTICS EXPRESS 7496

Optics EXPRESS

Synthesis of discrete phase-coherent optical spectra from nonlinear ultrasound

IVAN S. MAKSYMOV* AND ANDREW D. GREENTREE

ARC Centre of Excellence for Nanoscale BioPhotonics, School of Science, RMIT University, Melbourne, VIC 3001, Australia
*ivan.maksymov@rmit.edu.au

Abstract: Nonlinear acoustic interactions in liquids are effectively stronger than nonlinear optical interactions in solids. Thus, harnessing these interactions will offer new possibilities in the design of ultra-compact nonlinear photonic devices. We theoretically demonstrate a new scheme for synthesis of optical spectra from nonlinear ultrasound harmonics using a hybrid liquid-state and nanoplasmonic device compatible with fibre-optic technology. The synthesised spectra consist of a set of equally spaced optical Brillouin light scattering modes having a well-defined phase relationship between each other. We suggest that these spectra may be employed as optical frequency combs whose spectral composition may be tuned by controlling the nonlinear acoustic interactions.

OCIS codes: (250.5403) Plasmonics; (310.6628) Subwavelength structures, nanostructures; (230.1040) Acousto-optical devices.

References and links

1. J.-C. Diels and W. Rudolph, *Ultrashort Laser Phenomena: Fundamentals, Techniques, and Applications on a Femtosecond Time Scale* (Academic, 1996).
2. V. Torres-Company and A. M. Weiner, "Optical frequency comb technology for ultra-broadband radio-frequency photonics," Laser Photonics Rev. **8,** 368–393 (2014).
3. J. Faist, G. Villares, G. Scalari, M. Rösch, C. Bonzon, A. Hugi, and M. Beck, "Quantum cascade laser frequency combs," Nanophotonics **5,** 272–291 (2016).
4. A. A. Savchenkov, A. B. Matsko, and L. Maleki, "On frequency combs in monolithic resonators," Nanophotonics **5,** 363–391 (2016).
5. T. J. Kippenberg, R. Holzwarth, and S. A. Diddams, "Microresonator-based optical frequency combs," Science **332,** 555–559 (2011).
6. P. Del'Haye, K. Beha, S. B. Papp, and S. A. Diddams, "Self-injection locking and phase-locked states in microresonator-based optical frequency combs," Phys. Rev. Lett. **112,** 043905 (2014).
7. Q. Lu, S. Liu, X. Wu, L. Liu, and L. Xu, "Stimulated Brillouin laser and frequency comb generation in high-Q microbubble resonators," Opt. Lett. **41,** 1736–1739 (2016).
8. A. A. Savchenkov, A. B. Matsko, V. S. Ilchenko, D. Seidel, and L. Maleki, "Surface acoustic wave opto-mechanical oscillator and frequency comb generator," Opt. Lett. **36,** 3338–3340 (2011).
9. P. Del'Haye, A. Coillet, W. Loh, K. Beha, S. B. Papp, and S. A. Diddams, "Phase steps and resonator detuning measurements in microresonator frequency combs," Nat. Commun. **6,** 5668 (2015).
10. T. Herr, V. Brasch, J. D. Jost, C. Y. Wang, N. M. Kondratiev, M. L. Gorodetsky, and T. J. Kippenberg, "Temporal solitons in optical microresonators," Nat. Photonics **8,** 145–152 (2014).
11. M. Kauranen and A. V. Zayats, "Nonlinear plasmonics," Nat. Photonics **6,** 737–748 (2012).
12. B. J. M. Hausmann, I. Bulu, V. Venkataraman, P. Deotare, and M. Lončar, "Diamond nonlinear photonics," Nat. Photonics **8,** 369–374 (2014).
13. I. S. Maksymov, A. E. Miroshnichenko, and Yu. S. Kivshar, "Cascaded four-wave mixing in tapered plasmonic nanoantenna," Opt. Lett. **38,** 79–81 (2013).
14. X. Y. Z. Xiong, L. J. Jiang, W. E. I. Sha, Y. H. Lo and W. C. Chew, "Compact nonlinear Yagi-Uda nanoantennas," Sci. Rep. **6,** 18872 (2016).
15. N. Maccaferri, K. E. Gregorczyk, T. V. A. G. de Oliveira, M. Kataja, S. van Dijken, Z. Pirzadeh, A. Dmitriev, J. Åkerman, M. Knez, and P. Vavassori, "Ultrasensitive and label-free molecular-level detection enabled by light phase control in magnetoplasmonic nanoantennas," Nat. Commun. **6,** 6150 (2015).
16. I. L. Fabelinskii, *Molecular Scattering of Light* (Springer, 1968).
17. S. N. Gurbatov, O. V. Rudenko, and C. M. Hedberg, *Nonlinear Acoustic Through Problems and Examples* (Trafford, 2009).
18. M. Wegener, *Extreme Nonlinear Optics: An Introduction* (Springer, 2005).

#284744 https://doi.org/10.1364/OE.25.007496
Journal © 2017 Received 13 Jan 2017; revised 7 Feb 2017; accepted 7 Feb 2017; published 23 Mar 2017

Optics EXPRESS

19. Z.-F. Peng, W.-J. Lin, S.-L. Liu, C. Su, H.-L. Zhang, and X.-M. Wang, "Phase relation of harmonics in nonlinear focused ultrasound," Chin. Phys. Lett. **33,** 084301 (2016).
20. M. F. Hamilton, V. A. Khokhlova, and O. V. Rudenko, "Analytical method for describing the paraxial region of finite amplitude sound beams," J. Acoust. Soc. Am. **101,** 1297–1308 (1997).
21. T. Khokhlova, A. Maxwell, W. Kreider, V. Khokhlova, M. O'Donnell, and O. Sapozhnikov, "A method for phase aberration correction of high intensity focused ultrasound fields using acoustic nonlinearity," J. Acoust. Soc. Am. **140,** 3083 (2016).
22. Z. Meng, V. V. Yakovlev, and Z. Utegulov, "Surface-enhanced Brillouin scattering in a vicinity of plasmonic gold nanostructures," Proc. SPIE **9340,** 93400Z (2015).
23. I. S. Maksymov and A. D. Greentree, "Plasmonic nanoantenna hydrophones," Sci. Rep. **6,** 32892 (2016).
24. E. Eunjung Jung and D. Erickson, "Continuous operation of a hybrid solid-liquid state reconfigurable photonic system without resupply of liquids," Lab Chip **12,** 2575–2579 (2012).
25. C. L. Phillips, E. Jankowski, B. Jyoti Krishnatreya, K. V. Edmond, S. Sacanna, D. G. Grier, D. J. Pine, and S. C. Glotzer, "Digital colloids: reconfigurable clusters as high information density elements," Soft Matter **10,** 7468–7479 (2014).
26. T. Krupenkin, S. Yang, and P. Mach, "Tunable liquid microlens," Appl. Phys. Lett. **82,** 316–318 (2003).
27. R. Altkorn, I. Koev, R. P. Van Duyne, and M. Litorja, "Low-loss liquid-core optical fiber for low-refractive-index liquids: fabrication, characterization, and application in Raman spectroscopy," Appl. Opt. **36,** 8992–8998 (1997).
28. P. C. Scholten, "The origin of magnetic birefringence and dichroism in magnetic fluids," IEEE Trans. Magnet. **MAG-16,** 221–225 (1980).
29. V. I. Stepanov and Yu. L. Raikher, "Dynamic birefringence in magnetic fluids with allowance for mechanical and magnetic degrees of freedom of the particles," J. Magn. Magn. Mater. **252,** 180–182 (2002).
30. I. S. Maksymov, "Magneto-plasmonic nanoantennas: basics and applications," Rev. Phys. **1,** 36–51 (2016).
31. J. Wu. D. Xiang and R. Gordon, "Characterizing gold nanorods in aqueous solution by acoustic vibrations probed with four-wave mixing," Opt. Express **24,** 12458–12465 (2016).
32. D. Guo, G. Xie, and J. Luo, "Mechanical properties of nanoparticles: basics and applications," J. Phys. D Appl. Phys. **47,** 013001 (2014)
33. K. O'Brien, N. D. Lanzillotti-Kimura, J. Rho, H. Suchowski, X. Yin, and X. Zhang, "Ultrafast acousto-plasmonic control and sensing in complex nanostructures," Nat. Commun. **5,** 4042 (2014).
34. W.-S. Chang, F. Wen, D. Chakraborty, M.-N. Su, Y. Zhang, B. Shuang, P. Nordlander, J. E. Sader, N. J. Halas, and S. Link, "Tuning the acoustic frequency of a gold nanodisk through its adhesion layer," Nat. Commun. **6,** 7022 (2015).
35. R. Fleury, A. B. Khanikaev, and A. Alù, "Floquet topological insulators for sound," Nat. Commun. **7,** 11744 (2016).
36. D. Rossing, *Spinger Handbook of Acoustics* (Springer, 2007).
37. A. A. Maznev and O. B. Wright, "Upholding the diffraction limit in the focusing of light and sound," arXiv:1602.07958.
38. T. G. Leighton, *The Acoustic Bubble* (Academic, 1994).

1. Introduction

An optical frequency comb (OFC) is a spectrum consisting of a series of discrete, equally spaced elements that have a well-defined phase relationship between each other (for a review see, e.g., [1–4]). OFCs are important in precision measurements, microwave generation, telecommunications, astronomy, spectroscopy and imaging. They are usually produced by using mode-locked lasers or exploiting nonlinear (NL) optical effects in optical fibres.

Integrated NL optics [4–7] and optomechanics [8] also allow generating OFCs in microphotonic systems. However, the existing sources of microresonator OFCs (microcombs) have a number of limitations that motivate the ongoing research efforts. In OFCs based on femtosecond mode-locked lasers, all the modes are forced to have an equal phase, which implies that in the time domain the waves of different frequency will add constructively at one point resulting in a train of intense and short optical pulses [1]. In contrast to mode-locked laser combs, the generation principle of microcombs is based on a cascade of four-wave mixing processes in a high quality factor microresonator and does not utilise conventional laser emission [4–7]. Consequently, there is still no consensus on possible mode-locking mechanisms in microcombs that could re-enforce the equal spacing between the modes and align the phases to generate ultrashort optical pulses [6, 9]. As a result, new mechanism for OFC synthesis are required, such as the generation of solitons in microresonators that leads to a spontaneous phase-alignment [10].

Nanoscale OFC sources will be required for applications in nanophotonic circuits, but they

Optics EXPRESS

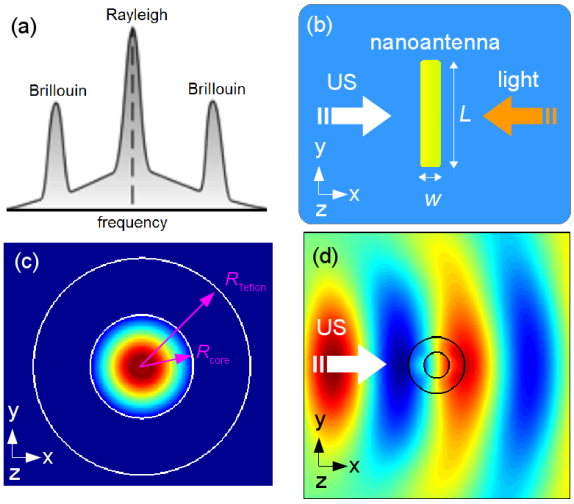

Fig. 1. (a) Sketch of a typical BLS spectrum. (b) Schematic of a nanorod NA immersed into water and insonated by ultrasound (US). The direction of propagation of light is shown schematically for the case of a standalone NA, and it has to be along the z-axis when the NA operates inside the water-filled fibre shown in (c, d). The wavelength of ultrasound is two orders of magnitude larger than the width $w = 30$ nm and length $L = 340$ nm of the NA. The E-field of the optical plane wave incident on the NA is polarised along the y-coordinate. (c) $|E|$-field intensity in the cross-section of the water-filled core ($R_{\text{core}} = 250$ μm) fibre with a Teflon coating ($R_{\text{Teflon}} = 525$ μm). The fibre is surrounded by water. The optical frequency is 405 THz. (d) Instantaneous time-domain snapshot of the T_{xx} stress component in the cross-section of the fibre and surrounding water. Note that the incident ultrasound wavefront is almost unchanged by the fibre. The frequency of ultrasound is 10 MHz.

are even more difficult to demonstrate than their microphotonic counterparts. Firstly, their development faces the same challenges as in the case of microphotonic systems [4–7, 9]. Secondly, whereas NL optical effects may, in general, be enhanced using ultra-small metal nanostructures [11], the generation of OFCs at the nanoscale is impeded by high absorption, short NL interaction lengths, phase matching challenges, and other fundamental limitations.

These limitations can be mitigated by capitalising on the advances in NL diamond nanophotonics [12] and plasmonic nanoantennae (NAs) [13, 14]. For example, an OFC may be generated with a tapered multielement NA designed such that its elements resonate at one of the comb frequencies [13], but the phase of each resonant mode is additionally controlled using one of the available methods [15]. However, tapered NAs have a relatively large metal volume, which decreases the NL generation efficiency because of absorption and heating. On the other hand, diamond combines a high refractive index, low absorption losses and excellent thermal properties attractive for integrated NL photonics [12]. However, its optical nonlinearities have not yet been fully studied, but the footprint of diamond-based devices remains in the range of several hundreds of square microns [12]. Thus, the search for new nanoscale OFC sources remains open.

In this paper, we exploit NL acoustic interactions in liquids instead of conventional NL optical interactions in solids, and we theoretically demonstrate a new scheme for synthesis of optical spectra consisting of a set of equally spaced modes having an aligned phase. Both the equal spacing between the modes and the phase alignment are achieved by controlling the generation of NL ultrasound waves in liquids and converting the corresponding acoustic spectra into optical ones through plasmonic NA-enhanced Brillouin Light Scattering (BLS) from ultrasound [16].

Optics EXPRESS

We suggest that these unique properties will allow employing the proposed spectrum synthesis scheme in novel nanoscale sources of OFCs.

Our interest in light scattering from NL acoustic waves is mostly motivated by the fact that NL acoustic interactions in liquids [17] are effectively stronger than NL optical interactions in solids. The propagation of the incident ultrasound with frequency f_{us} in an acoustically NL medium gives rise to higher harmonics with frequencies $n f_{us}$ (n is a positive integer). In contrast to NL optics where the generation of the higher ($n > 5$) harmonics is often difficult to observe, acoustic harmonics with n up to ~ 15 are readily achievable [17].

The strength of NL acoustic interactions in liquids is quantified by the NL acoustic coefficient $\beta = (\gamma + 1)/2 = 1 + B/2A$, where γ is the heat capacity ratio the use of which for liquids is justified in [17] and references therein, and A and B are the expansion factors of a series that represents the pressure fluctuations $p' = A(\rho'/\rho) + (B/2)(\rho'/\rho)^2 + \ldots$ in terms of the density increment ρ' [17].

Many liquids have a large β. For example, water has $\beta = 3.5$, optically transparent oils have $\beta \approx 6$, but water with bubbles has $\beta \approx 5000$ [17]. It is noteworthy that β of liquids increases as the temperature is increased, which opens up opportunities to control the strength of NL acoustics interactions. Moreover, an extremely high β of water with bubbles has no direct analogues in NL optics, including extreme NL optics [18].

The spectrum of light scattered from single-frequency incident ultrasound with frequency f_{us} has a form of a triplet [Fig. 1(a)], consisting of the central Rayleigh mode and two BLS modes shifted by $\pm f_{us}$ with respect to the Rayleigh mode [16]. In the presence of both incident ultrasound and its NL-generated harmonics, the BLS spectrum exhibits multiple, equally spaced modes at $\pm n f_{us}$, which implies that the spacing between the modes is controllable at will by changing f_{us}. Significantly, a simplified but practically feasible theory of one-dimensional NL acoustic plane waves [17, 19] predicts that the fundamental and higher order harmonics of ultrasound will have the same phase because no diffraction occurs. This property leads to a spontaneous phase alignment between the optical BLS modes. Should an even stronger NL acoustic interaction be desired, an acoustic lens may be used to focus ultrasound. Of course the focusing of ultrasound leads to phase shifts of the harmonics due to diffraction [19, 20]. However, such phase shifts can be compensated [21] to maintain the phase alignment between the corresponding BLS optical modes.

Nevertheless, despite the possibility to attain high ultrasound pressures and strong NL acoustic effects, the optical intensity of the BLS modes corresponding to the higher acoustic harmonics remains low due to the fundamentally weak interaction of light with ultrasound [16]. Thus, to be employed as a source of OFCs, the intensity of the optical BLS modes has to be increased. It has recently been shown that the strength of the interaction of light with single-frequency ultrasound is increased by using plasmonic nanostructures such as plasmonic grating and NAs [22, 23]. Therefore, we capitalise on the previous results and demonstrate that the intensity of all BLS modes in the spectrum can be increased by using an ultra-small, single-element plasmonic NA.

2. Results and discussion

We consider a single, square cross-section silver nanorod NA with a $30 \times 340 \times 30$ nm^3 volume [Fig. 1(b)]. The NA is surrounded by water with refractive index $n_{water} = 1.33$, NL acoustic parameter $\beta_{water} = 3.5$, density $\rho = 1000$ kg/m^3 and speed of sound $c_0 = 1500$ m/s [23]. Because the majority of optically transparent liquids have $\beta \approx \beta_{water}$ [17], results presented below will hold for other liquids including oils.

At present there are a number of technological challenges that prevent the practical integration of liquid-state elements into traditional solid-state microphotonic systems [24, 25]. However, liquid-state devices offer a number of potentially transformative advantages for

Optics EXPRESS

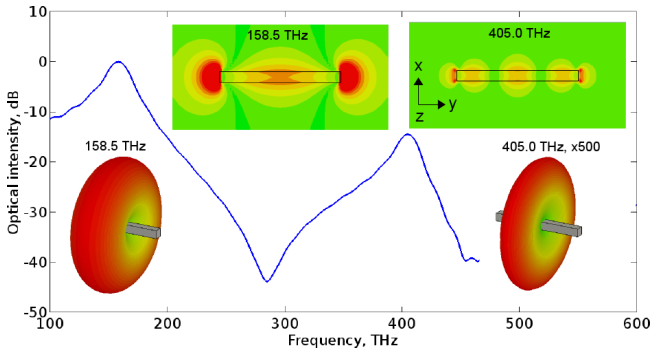

Fig. 2. Optical properties of the NA. The insets show the near-field $|E_y|$-field profiles (top) and far-field power profile (bottom) corresponding to the fundamental (158.5 THz) and higher-order (405 THz) modes. The far-field power profile of the higher-order mode is multiplied by 500.

microphotonic systems [24, 25]. Successful examples include liquid-state optical lenses [26] and liquid-core optical fibres [27].

Consequently, we first discuss a strategy for the integration of this NA with optical fibres. We propose to use a liquid core optical fibre [27], which may host the NA inside the core. Because simultaneous plasmonic-opto-acoustic simulations of this scenario are computationally impractical, we first model optical and acoustic properties of the fibre without the NA. By considering a Teflon water-core fibre ($n_{\text{Teflon}} = 1.29$ [27], $\rho = 2200$ kg/m^3, $c_0 = 1400$ m/s and shear wave speed 440 m/s) we show that the fibre may operate in water [Fig. 1(c)]. We also show that a good agreement between the characteristic specific acoustic impedance ($z_0 = \rho c_0$) of Teflon and water makes this fibre mostly transparent to ultrasound propagating in the direction perpendicular to the fibre core [Fig. 1(d)]. The optical and elastic finite-difference time-domain (FDTD) methods [23] were used to obtain the results in Figs. 1(c) and 1(d).

The general problem of controlled nanoparticle or NA orientation in a liquid solution remains unsolved. Thus, inside the liquid core of the fibre, the main axis of the NA may not necessarily coincide with the direction of propagation of light and ultrasound schematically shown in Fig. 1. However, we may employ many identical NA's. In that case, only those NA's that happen to orientate in the right direction will be excited by the incident light and will contribute to the interaction of light with ultrasound. Alternatively, in a fashion similar to controlled nanoparticle orientation in magnetic fluids [28, 29], we may apply external magnetic fields to control the orientation of magneto-plasmonic NA's (for a review see, e.g., [30]). The latter approach should also work in the case of a single NA.

3D simulations with CST Microwave Studio software reveal that in the 100−500 THz spectral range the spectrum of the NA [Fig. 2(a)] has the fundamental mode and one higher-order mode. In [23] we established that the results of 3D simulations are qualitatively reproduced by 2D simulations, with the major difference being a blueshift of all resonance peaks with respect to the 3D case, because the nanorod is modelled as a plate.

The NA tuned on the higher-order mode radiates lower power into the far-field zone (bottom insets in Fig. 2) as compared with the fundamental mode. This is attributed [23] to a Fabry-Perot behaviour and strong near-field zone (top insets) confinement of light to the NA surface.

The dielectric permittivity of water and silver are modulated because of alternating density changes caused by ultrasound pressure. In bulk water, light may reliably sense these changes only when the optical wave propagates over macroscopically long distances and interacts with hundreds of periods of modulation [16]. Consequently, the interaction of light with ultrasound

Optics EXPRESS

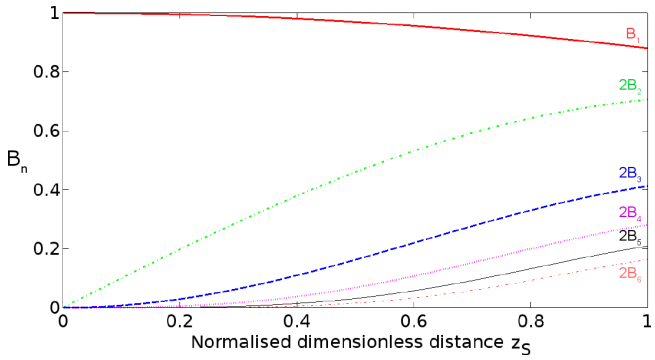

Fig. 3. Distance-dependent amplitudes of the first six harmonics of an initially sinusoidal ultrasound wave. The second and higher harmonic amplitudes are multiplied by 2 for the sake of visualisation, because they are small as compared with the amplitude of the fundamental harmonic.

in microscopically small volumes of water is very weak. Indeed, the diameter of the water-filled core of the optical fibre equals to ~ 3 (~ 33) periods of modulation corresponding to the 10 MHz (100 MHz) incident ultrasound. Furthermore, when it is required to employ a single NA without the fibre, the volume of water around the NA may be reduced up to ~ 1 μm^3. However, this implies that without the NA in this volume of water the interaction of light with ultrasound will be negligibly small.

At the same time, when the NA is employed, light becomes tightly confined to the metal surface of the NA and its interaction with ultrasound in the same small volume of water dramatically increases. This increase is mostly possible because of the Fabry-Perot behaviour of the higher-order mode of the NA, but the operation of the NA at the fundamental mode does not produce any significant improvement as compared with the case of bulk water [23].

We solve the Earnshaw equation to analyse the weak NL acoustic interaction in a liquid [17].

$$\frac{\partial^2 \xi}{\partial t^2} = c_0^2 \frac{\partial^2 \xi / \partial x^2}{(1 + \partial \xi / \partial x)^{\gamma+1}}. \tag{1}$$

where c_0 is the speed of sound in the liquid and $|\partial \xi / \partial x| << 1$. We expand the term $(1 + \partial \xi / \partial x)^{-(\gamma+1)}$ into the binomial series and employ the method of slowly varying envelope to find a solution in the form of two arbitrary travelling waves $\xi = \Phi(t - x/c_0) + \Psi(t + x/c_0)$. We consider only the wave travelling in the positive direction. The wave profile changes slowly leading to $\xi = \Phi(\tau = t - x/c_0, x_1 = \mu x)$, where $\mu << 1$.

We obtain the simple wave equation $\frac{\partial u}{\partial x} = \frac{\beta}{c_0^2} u \frac{\partial u}{\partial \tau}$, where $u = \partial \xi / \partial \tau$ is the particle velocity and β is the NL acoustic coefficient. In the following, β enters the expression for the normalised dimensionless distance $z_S = (\beta / c_0^2) \omega u_0 x = x / x_S$, where $\omega = 2\pi f_{us}$ and x_S is the acoustic wave discontinuity formation length [17]. We use the Fourier series expansion to derive the relationship between the harmonic amplitude u and the amplitude of the incident ultrasound wave u_0 as a function of z_S. Then we calculate the expansion coefficients by using the nth-order Bessel functions of the first kind to arrive to the Bessel-Fubini solution

$$\frac{u}{u_0} = \sum_{n=1}^{\infty} B_n(z_S) \sin(n\omega\tau), \tag{2}$$

where $B_n(z_S) = 2J_n(nz_S)/(nz_S)$ are the harmonic amplitudes. Figure 3 shows the dependencies of the first six harmonic amplitudes of ultrasound on the distance z_S. At $z_S = 1$ these waves

Optics EXPRESS

carry ~ 98% of the total acoustic energy, with the remainder being carried by the higher-order harmonics. It is noteworthy that the model predicts that all harmonics have the phase $\theta = 0$ because no diffraction occurs in the considered scenario of one-dimensional plane wave propagation [17, 19].

However, we are also interested in the scenario of NL acoustic interaction of ultrasound waves focused by an acoustic lens. In this case, NL phenomena often give rise to phase shifts of the harmonic waves introduced by the diffraction [20]. Both theory and experiment show that at the focus the relative phase of nth ultrasound harmonic approximately equals $(n-1)\pi/3$ [19]. In general, this phase shift is undesirable because it may result in a respective phase shift of the optical BLS modes. In the following we assume that this phase shift is compensated such that θ is constant for all harmonics by using one of the available methods [21].

The result presented in Fig. 3 is valid for a broad range of frequencies f_{us} [16]. Nevertheless, in our analysis we keep the maximum value of f_{us} such that the frequency of the 10th harmonic remains below ~ 1 GHz, which is the frequency above which the NA may resonantly vibrate [31]. By using Eq. (1) from [31] and the material parameters of silver from [23] (and noting that the Young's modulus for nanoparticles may be different from the bulk material [32]), we calculate that the frequency of the fundamental extensional mode of the NA equals ~ 4.14 GHz.

Vibrations at the fundamental and higher-order elastic mode frequencies may lead to interesting effects, including the generation of OFCs [5, 7]. However, in this work we are mainly interested in the operation of the NA below its structural resonances – i.e., the quasi-static regime. The operation in this regime will ensure that all acoustic signals originate from the NL acoustic interactions in water and thus have a well-defined line width, intensity and phase relationship. These requirements are crucial for the generation of phase-coherent optical spectra (see below), but they will be challenging to meet if the NA resonantly vibrate in addition to the NL acoustic interactions in water. Indeed, the line width, intensity and phase of the NA vibrational modes will depend on the type and number of the mode [31], which is an undesirable effect for our study.

In contrast to quite well researched resonant structural deformations of plasmonic nanostructures such as nanorods, discs, crosses, etc. [31, 33, 34], studies of the quasi-static regime are rarely encountered in the literature and difficult to model [23]. In the quasi-static regime, the NL acoustic effects are unaffected by the NA [23]. The NA is considered as a bulk medium, the normal stress components are equal to the ultrasound pressure P taken with the opposite sign, and the shear stress is zero. From Hooke's law we define the strain components, which are used to calculate the displacement $\boldsymbol{s}$ and the respective variations $\Delta\epsilon$ of the dielectric permittivity of water and silver due to the ultrasound pressure [23].

To synthesise an optical spectrum we have to employ high-intensity ultrasound to produce as high as possible acoustic intensities of NL harmonics. However, for the presented NL acoustic theory to be exact we have to maintain $\mu << 1$ (i.e. the acoustic Mach number $M = u_0/c_0 << 1$), which restricts the maximum value of the pressure that we can choose. Thus, as a trade-off, in the following we assume that $P = 500$ MPa, which corresponds to $M \approx 0.2$ for which we expect our model to remain mostly valid.

For $P = 500$ MPa we obtain the changes of the dielectric permittivity of silver $\Delta\epsilon_{\mathrm{Ag}} = 0.02$ and water $\Delta\epsilon_{\mathrm{water}} = 0.0035$ (see [23] for details). The stress also leads to the compression of the NA with a decrease in its length and width $\Delta L \approx 0.5$ nm and $\Delta w \approx 0.05$ nm. Whereas the changes in the dielectric permittivity can be modelled, simulations of the NA undergoing periodic deformations are challenging when using any technique relying on the discretisation with a mesh.

However, as long as linearity holds and Hooke's law remains valid, changes in the volume of the NA may be modelled by changing the compressibility of the constituent material [35]. In our optical simulations, the role of the compressibility is played by the dielectric permittivity

Optics EXPRESS

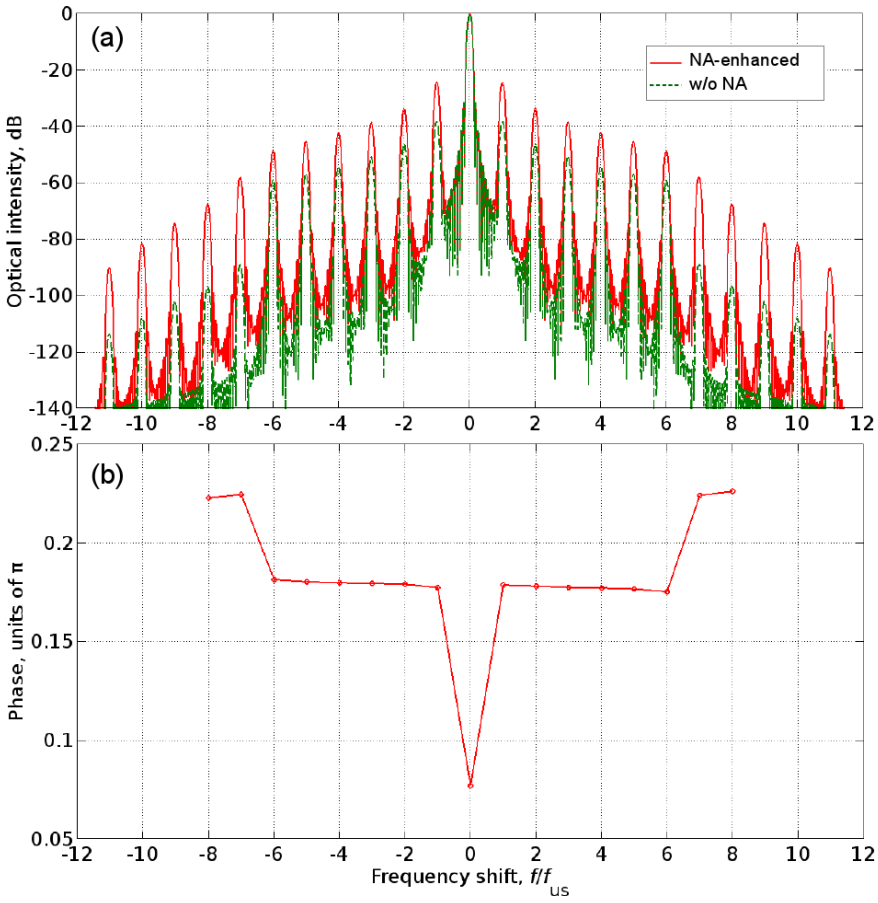

Fig. 4. (a) Optical spectra synthesised from NL ultrasound by the BLS effect. The optical intensity is shown as a function of the frequency shift with respect to 405 THz (the frequency of incident light), normalised to the frequency f_{us} of the incident ultrasound. Red solid line: NA-enhanced spectrum. Green dashed line: without the NA. (b) Phase corresponding to the peaks of the NA-enhanced spectrum. Note a small change of the phase when viewed at the $-\pi$ to π scale. The solid line is the guide to the eye only. Note that the phase of the ninth and higher modes could not be extracted, as explained in the main text.

of silver ϵ_{Ag}, which is given by the Drude model [23]. The changes in the volume of the NA are taken into account by a factor $\Delta\epsilon_{\mathrm{vol}}$. In a single CST Microwave Studio simulation run, we obtain the optical spectrum of the NA with a static volume updated using the values of ΔL and Δw and observe a very small but routinely detectable shift in the resonance peak. Then we repeat the simulation for the unperturbed volume NA but vary the value of $\Delta\epsilon_{\mathrm{vol}}$ to obtain the same spectral shift as in the first simulation. We find $\Delta\epsilon_{\mathrm{vol}} = -0.005$ that is four times smaller than $\Delta\epsilon_{\mathrm{Ag}}$ and its sign is opposite to that of $\Delta\epsilon_{\mathrm{Ag}}$. This implies that the deformation of the NA will decrease the strength of the BLS effect, which is a physical result because a decrease in the volume of the NA leads to a smaller overlap of the near field of the NA with the surrounding medium.

We use a 2D optical FDTD method [23] to demonstrate the synthesis of a discrete optical spectrum from NL ultrasound [Fig. 4(a)]. The first six BLS modes to the left and right of the central, unshifted with respect to the frequency of incident light (405 THz) mode correspond to the six ultrasound harmonics (Fig. 3) and they are enhanced by the NA [red solid line

Optics EXPRESS

in Fig. 4(a)] with respect to the case of bulk water (green dashed line) used as a reference. Moreover, as established in our case, the cascaded BLS effect leads to the generation of the seventh, eighth and so on harmonics seen both in the spectra with and without the NA. Without the NA the intensity of these harmonics quickly drops, but their decrease is significantly less steep in the presence of the NA.

The origin of the cascaded BLS effect was verified by means of simulation in which only the fundamental ultrasound harmonic was retained but the NL acoustic interactions were artificially turned off by setting $\beta = 0$. Apart from the expected BLS modes due to ultrasound at f_{us}, we also observed two additional BLS modes corresponding to the frequency $2f_{\mathrm{us}}$. This is because the BLS modes due to ultrasound at f_{us} played the role of the secondary incident light signals and the Brillouin scattering of these signals from ultrasound resulted in additional BLS modes at $2f_{\mathrm{us}}$. The intensity of these additional BLS modes is very low because the intensity of the secondary incident light is itself very low.

From the simulated results we also extract the phase at the frequencies corresponding to the central Rayleigh mode and the first eight BLS modes in Fig. 4(a). Unfortunately, we were unable to extract the phase of the ninth, tenth and so on modes due to numerical artefacts associated with small reflections from the boundaries of the computational domain and a very low optical intensity of these modes. However, this limitation does not interfere with our further analysis.

As shown in Fig. 4(b), all the modes have a nearly aligned phase, which is a feature required for the synthesis of an OFC. One can see that the phase of the central, unshifted mode of the spectrum is different from that of the first six modes that are frequency-shifted to the left and to the right from the centre. In turn, the phase of the seventh and eighth modes does not follow the trend exhibited by the phase of the first six modes. We explain these differences below.

The central, unshifted peak of the spectrum corresponds to the Rayleigh scattering mode. Similar to Brillouin scattering, Rayleigh scattering is also due to fluctuations in the density of the transmitting medium, and hence of its dielectric permittivity. However, Rayleigh scattering involves only random and incoherent thermal fluctuations, in contrast with correlated, periodic fluctuations that cause Brillouin scattering [16]. Consequently, the phase of the Rayleigh mode differs by $\sim 0.1\pi$ from that of the BLS modes. However, this difference is small as compared with discrete $\pi/2$ or π phase steps that are undesirable in the generation of microcombs by a cascade of four-wave mixing processes [9].

Brillouin scattering can be explained by considering the Doppler shift [16]. The fluctuations in the dielectric permittivity caused by ultrasound give rise to a moving grating that scatters the incident light with a Doppler effect producing a shifted Doppler frequency $f_{\mathrm{D}} = -(2\pi)^{-1}\Delta\theta/\Delta t$, where $\theta = 4\pi r/\lambda$ is the Doppler phase defined by the distance r travelled by light between the centre of the NA and the moving grating, and λ is the wavelength of light.

The NA senses ultrasound mostly by its surface and thus the distance $r \approx \frac{w}{2} + \Delta r$, where w is the width of NA and Δr accounts for the fluctuations in the dielectric permittivity caused by ultrasound. When $\Delta r = 0$, we estimate that all BLS modes should have a phase offset of $\sim 0.12\pi$. This value is in good agreement with the simulated phase offset $\sim 0.17\pi$ [Fig. 4(b)]. Furthermore, the simulation demonstrates that the phase of the BLS modes slightly lags (leads) with respect to the offset value when $\Delta r > 0$ ($\Delta r < 0$). This is because the effective distance r increases (decreases) leading to a negative (positive) frequency shift. This picture holds for the modes with the normalised frequency shift in the range from ± 1 to ± 6, in which the phase exhibits a slightly asymmetric profile with respect to the zero frequency shift [Fig. 4(b)].

However, the phase pattern corresponding to the seventh and eight BLS modes exhibits a more complex behaviour. Recall that in our model we force the excitation of the first six ultrasound harmonics only and we control the phase of the corresponding optical BLS modes. In contrast, the appearance of the seventh and eight BLS modes is attributed to the cascaded BLS effect and the corresponding phase is no longer fixed but shifted by $\sim 0.05\pi$. However,

Optics EXPRESS

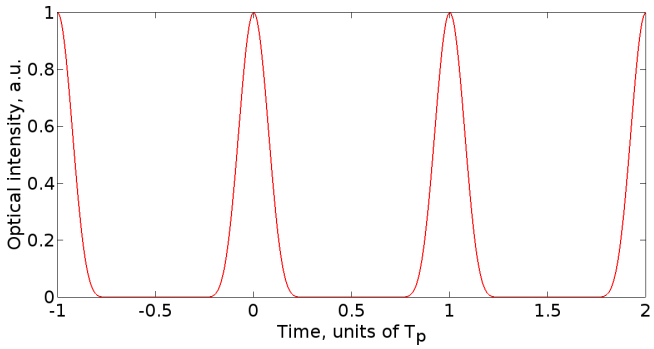

Fig. 5. Fourier transformation of the BLS mode spectrum shown in Fig. 4. The time scale is given in the units of $T_p = 1/\delta$, where δ is the frequency spacing between the BLS modes.

this difference is also small when viewed at the scale of $\pi/2$ or π phase steps.

Because all the modes of the spectrum in Fig. 4(a) have a quasi-aligned phase, similar to mode-locked OFCs in the time domain the modes of different frequency should add constructively at one point resulting in a train of optical pulses spaced by $T_p = 1/\delta$, where δ is the frequency spacing between the BLS modes. However, when the modes have a random phase distribution, instead of a train of well-defined pulses one should obtain a noise-corrupted signal. This physical mechanism is schematically illustrated in Fig. 5.1 of [1].

We simulate this physical picture by Fourier-transforming the spectrum in Fig. 4 and obtaining time-domain optical intensity signals. Because in our model the frequency spacing δ between the BLS modes is given in the normalised frequency shift f/f_{us} units, for the sake of generality the time axis of the resulting time-domain optical intensity is presented in units of $T_p = 1/\delta$ corresponding to the duration of one pulse train. We also make use of the periodic nature of the Fourier transformation to show several periods of the pulse train. The Fourier transformation of the data in Fig. 4 produces well-defined single optical pulses (Fig. 5).

3. Conclusions

We have shown that harnessing strong NL acoustic interactions in liquids offers new possibilities in the design of ultra-compact, fibre-optic compatible sources of discrete and phase-coherent optical spectra. Through simulations we have demonstrated that these sources may be employed to generate OFCs, which are similar, for example, to microcombs with a quasi-triangular (in the log scale) spectral lines produced via hyper-parametric oscillation processes [4]. The number of spectral lines obtained with the proposed OFC source is higher as compared with discrete spectra that may be produced by means a cascade of NL-optical four-wave mixing processes in a tapered NA [13]. However, the footprint of the proposed source is much smaller than that of tapered NAs and similar plasmonic nanostructures such as subwavelength gratings [22]. Furthermore, we have shown that the spacing between the lines of the spectrum synthesised from ultrasound can be controlled at will by changing the frequency and intensity of incident ultrasound or by controlling the NL acoustic parameter of the liquid.

In a NL optical medium, broader and flatter combs may be achieved by mixing two triangular OFCs with different central wavelengths [2]. The same strategy remains applicable when the NL acoustic interactions are exploited. Here, two seed combs may be produced by using ultrasound at different frequencies and mixed in a NL acoustic medium, which will result in broader and flatter combs as compared with the result in Fig. 4.

A typical NL-optical source of microcombs has a cubic centimetre volume and operates at $\sim$ 20 – 100 mW of laser power [12], but the total consumed power is $\sim$ 1 W [4]. Because

Optics EXPRESS

NL optical interactions at the nanoscale are weaker than at the microscale, the power needs to be increased when the dimensions of the resonator are decreased towards the nanoscale. We estimate that the OFC source based on a single tapered NA will require at least 3 W of continuous wave laser power, which is a challenging requirement.

The proposed ultrasound-based OFC source does not need high laser power, but it demands ultrasound pressures of ~ 0.5 GPa. When the ultrasound focal area dimensions are only limited by the diffraction (half the wavelength) limit, we estimate that for the synthesis of the comb shown in Fig. 4 one needs the acoustic power of ~ 10 W at f_{us} = 100 MHz.

Acoustic power of up to ~ 1 kW is readily achievable with medical high-intensity focused ultrasound (HIFU) transducers that have a ~ 50% electrical-to-acoustic conversion efficiency [36]. Moreover, it has been shown that the focal area of the transducer may be reduced by using acoustic metamaterials, which allows focusing ultrasound into deep-subwavelength, 1/40 of the incident wavelength spots [37]. Thus, the required acoustic power may be decreased to ~ 20 mW.

High pressure ultrasound may also be produced by strong pulses emitted by collapsing gas bubbles in water [38]. The application of bubbles is attractive also because the NL acoustic parameter β of water with air bubbles is three orders of magnitude larger than that of without bubbles [17]. Such a high acoustic nonlinearity will result in stronger NL acoustic interactions and lower acoustic power required for the operation of the device.

Funding

This work was supported by Australian Research Council (ARC) through its Centre of Excellence for Nanoscale BioPhotonics (CE140100003) and LIEF program (LE160100051). This research was undertaken on the NCI National Facility in Canberra, Australia, which is supported by the Australian Commonwealth Government.